Rotating Polygon Instability of a Swirling Free Surface Flow

L. Tophøj,[1] J. Mougel,[2] T. Bohr,[1] and D. Fabre[2]

[1]*Physics Department and Center for Fluid Dynamics, Technical University of Denmark, 2800 Kongens Lyngby, Denmark*
[2]*Institut de Mécanique des Fluides de Toulouse, Université de Toulouse, 31400 Toulouse, France*
(Received 25 September 2012; published 8 May 2013)

We explain the rotating polygon instability on a swirling fluid surface [G. H. Vatistas, J. Fluid Mech. **217**, 241 (1990) and Jansson *et al.*, Phys. Rev. Lett. **96**, 174502 (2006)] in terms of resonant interactions between gravity waves on the outer part of the surface and centrifugal waves on the inner part. Our model is based on potential flow theory, linearized around a potential vortex flow with a free surface for which we show that unstable resonant states appear. Limiting our attention to the lowest order mode of each type of wave and their interaction, we obtain an analytically soluble model, which, together with estimates of the circulation based on angular momentum balance, reproduces the main features of the experimental phase diagram. The generality of our arguments implies that the instability should not be limited to flows with a rotating bottom (implying singular behavior near the corners), and indeed we show that we can obtain the polygons transiently by violently stirring liquid nitrogen in a hot container.

Experiments with a rotating free surface flow in a cylindrical container driven by a rotating bottom plate show the occurrence of spectacular polygonal patterns that rotate with essentially unchanged form [1,2]. Recent work [3] suggests that a linear instability of circular-symmetric "parent" states leads to asymmetric "children" states of polygon shape. Our starting point is thus the symmetric "parent" state sketched in Fig. 1(a). It was shown in Refs. [3,4] that, due to the secondary flows created by boundaries, the surface flow should be close to that of a potential vortex. It is also known that viscosity plays a minor role [2] and that indeed the flow is quite turbulent [5]. The bulk flow is thus not known in detail, and, due to the singularity near the corner C, where the rotating bottom plate meets the stationary sides, it must be quite complex. In this work, we shall neglect these complications and simply assume that the entire flow is that of a potential vortex with a dry core and that the perturbations around this flow remain potential. The success of this rough model implies that the singularity near C in Fig. 1 is not essential, and, indeed, we shall see that new and surprisingly simple experiments with stirred liquid nitrogen in a hot kitchen pot confirm that the polygon formation is a general feature of rapid swirling flows. Perturbations around a potential vortex flow were considered earlier in Ref. [6], but, since the treatment did not include the vertical dimension, no instability was found.

We describe the system using cylindrical (r, θ, z) coordinates. The unperturbed flow is that of a potential vortex with circulation Γ; i.e., the local flow velocity is in the azimuthal direction and has magnitude $U(r) = (\Gamma/2\pi r)$. We denote the inner radius of the fluid volume by ξ and the outer height by ζ [cf. Fig. 1(a)]. The shape of the fluid body in the unperturbed equilibrium state is determined by the

balance between the gravitational acceleration g and the centrifugal acceleration $U(r)^2/r$. On the free surface $z = z(r)$, the pressure is constant, and thus $g(\partial z/\partial r) = U(r)^2/r$, which yields

$$z(r) = \frac{1}{2g}\left(\frac{\Gamma}{2\pi R}\right)^2\left(\frac{R^2}{\xi^2} - \frac{R^2}{r^2}\right). \quad (1)$$

For comparison with the experiment, we shall keep the 3D fluid volume fixed. Calling H the height of liquid at rest (cf. Fig. 1), $\pi R^2 H = \int_\xi^R dr 2\pi r z(r)$ is the fluid volume, where $z(r)$ is given by (1). Thus, we can express $\zeta = z(R)$ and Γ in terms of H, ξ, and R:

$$\zeta = H\left(1 - 2\frac{\xi^2 \ln\frac{R}{\xi}}{R^2 - \xi^2}\right)^{-1}, \quad (2)$$
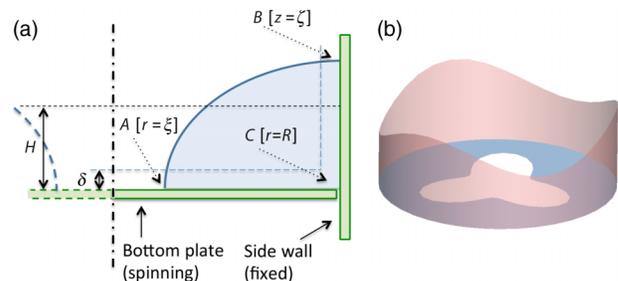
FIG. 1 (color online). Sketch of the setup and explanation of the 2D model. (a) Cross-sectional view, featuring the bottom plate and side walls, the actual volume occupied by the fluid (grey area) and a cut (ACB) through the domain considered in the simplified model. Initially, the cylindrical container of radius R is filled with water to height H. (b) 3D sketch of the 2D model displaying waves at its upper and inner surfaces.

$$\frac{\Gamma}{2\pi R} = \frac{\xi\sqrt{2gH}}{\sqrt{R^2 - \xi^2 - 2\xi^2 \ln\frac{R}{\xi}}}. \tag{3}$$

The free surface can support wave motions, which can be analyzed by adding small potential perturbations $\mathbf{v}' = \nabla\phi$ to the axisymmetric base flow. The potential ϕ satisfies the Laplace equation

$$\frac{\partial^2\phi}{\partial r^2} + \frac{1}{r}\frac{\partial\phi}{\partial r} + \frac{1}{r^2}\frac{\partial^2\phi}{\partial\theta^2} + \frac{\partial^2\phi}{\partial z^2} = 0, \tag{4}$$

and the kinematic and dynamic boundary conditions at the free surface can be combined to the single one:

$$\left(\frac{\partial}{\partial t} + \frac{U(r)}{r}\frac{\partial}{\partial\theta}\right)^2 \phi = -g_e \mathbf{n}\cdot\nabla\phi, \tag{5}$$

where $\mathbf{n}$ is the outward normal to the surface, and where $g_e = \sqrt{g^2 + [\Gamma^2/(4\pi^2 r^3)]^2}$ is the effective acceleration normal to the interface, combining gravity and centrifugal effects.

The linear problem (4) and (5) for the three-dimensional domain displayed in Fig. 1 has to be solved numerically. The solution is discussed below, but, prior to this, we investigate a simplified situation in which all the motion is assumed to take place in a two-dimensional domain lying along the boundaries, consisting of a planar annulus on the bottom [line AC in Fig. 1(a)] and a cylindrical surface along the side wall [line BC in Fig. 1(a)]. Physically, this domain can be thought of as a narrow channel of width δ, as if the flow was constricted by the presence of solid walls located at $z = \delta$ and $r = R - \delta$, as indicated by the dashed lines in Fig. 1(a). The eigenfunctions to (4) in the two parts of this domain have, respectively, the form

$$\phi_c = \left[K_1\left(\frac{r}{R}\right)^m + K_2\left(\frac{r}{R}\right)^{-m}\right]e^{i(m\theta - \omega t)}, \tag{6}$$

$$\phi_g = (K_3 e^{mz/R} + K_4 e^{-mz/R})e^{i(m\theta - \omega t)}, \tag{7}$$

where K_i are unknown constants, m is the azimuthal wave number, and $\omega = \omega_r + i\omega_i$, ω_r being the oscillation frequency and ω_i the growth rate. In the corner connecting the two subdomains, we assume continuity of pressure and conservation of flux:

$$\phi_c|_{C-} = \phi_g|_{C+}, \qquad \frac{\partial\phi_c}{\partial r}\bigg|_{C-} = \frac{\partial\phi_g}{\partial z}\bigg|_{C+}, \tag{8}$$

where $C-$ is the limit when approaching C from A ($r \to R$), and $C+$ is approaching C from B ($z \to 0$).

The free surface condition (5) applied at A and B then leads to

$$(\omega - m\Omega_\xi)^2\phi_c(\xi) = -g_c\frac{\partial\phi_c}{\partial r}\bigg|_{r=\xi}, \tag{9}$$

$$(\omega - m\Omega_R)^2\phi_g(\zeta) = g\frac{\partial\phi_g}{\partial z}\bigg|_{z=\zeta}, \tag{10}$$

where $\Omega_\xi = U(\xi)/\xi$ and $\Omega_R = U(R)/R$ are the rotation rates at A and B, and $g_c \equiv \Gamma^2/(4\pi^2\xi^3)$ is the centrifugal acceleration at the inner surface. Together with the corner conditions (8), which simply imply $K_1 = K_3$ and $K_2 = K_4$, they lead to a dispersion relation in the form

$$D_c(\omega)D_g(\omega) = \frac{m^2 g g_c}{\xi R}(F^2 - 1), \tag{11}$$

where

$$F = \frac{1 + e^{-2m\zeta/R}\left(\frac{\xi}{R}\right)^{2m}}{1 - e^{-2m\zeta/R}\left(\frac{\xi}{R}\right)^{2m}}, \tag{12}$$

$$D_c(\omega) = (\omega - m\Omega_\xi)^2 - g_c mF/\xi \tag{13}$$

$$D_g(\omega) = (\omega - m\Omega_R)^2 - gmF/R. \tag{14}$$

Since the term $(F^2 - 1)$ is a small quantity, especially in the large-m limit, Eq. (11) can be interpreted as describing the weak coupling of two kinds of waves. This situation is analogous to the three-layer model of the Kelvin-Helmholtz instability studied by Cairns [7]. In the present case, $D_g(\omega)$ and $D_c(\omega)$ are dispersion relations for two families of waves: "gravity waves" with frequency ω_g and "centrifugal waves" with frequency ω_c, which are obtained by considering the same set of equations but retaining only one of the free surface conditions: (10) for gravity waves and (9) for centrifugal ones [8]. Each of these wave types comes in two variants, depending on the sign chosen in (13) and (14), i.e., their direction of propagation compared to the local mean flow.

The full dispersion relation (11) is quartic in ω and is most conveniently solved numerically. Results are displayed in Fig. 2(a) for the case $H/R = 0.276$; $m = 3$. Away from the resonances, we get four solutions which are very close to the respective solutions of $D_g(\omega) = 0$ or $D_c(\omega) = 0$, i.e., the two gravity waves (where ω_g has a finite limit for $\xi \to 0$) and the two centrifugal waves (where ω_c diverges as $\xi \to 0$). Resonance occurs when the frequencies of the two kinds of waves coincide, i.e., $\xi/R \approx 0.43$ and $\xi/R \approx 0.78$. The first case is magnified in Fig. 2(b), which shows that, in a narrow range of ξ, the coupled problem displays two complex conjugate eigenvalues, one of them creating instability. The corresponding amplification rate is plotted in Fig. 2(c). On the other hand, the second case [magnified in Fig. 2(d)] does not give instability, since the two lines that appear to intersect in fact repel and the frequencies remain real throughout the interval.

These results are easy to understand, following the approach of Cairns [7]. Let us call ω_g and ω_c the respective solutions of $D_g(\omega) = 0$ or $D_c(\omega) = 0$ and suppose that they are close to resonance, i.e., $\omega_g = \omega_c + \epsilon$ with ϵ
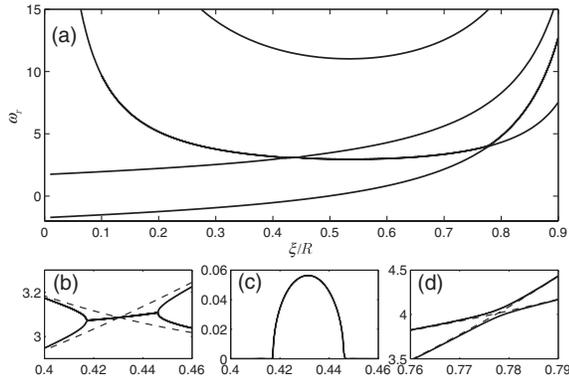
FIG. 2. Eigenvalues computed from the 2D model as function of ξ, for $H/R = 0.276$ and $m = 3$. (a) Oscillation frequencies ω_r. (b),(c) Magnifications around the unstable wave interaction at $\xi/R \approx 0.43$ displaying oscillation frequency ω_r and amplification rate ω_i. (d) Magnification of the stable wave interaction at $\xi/R \approx 0.78$. Thick lines represent solutions of the coupled model (11); thin lines represent solutions of the uncoupled model, i.e., roots of (13) and (14). All frequencies have been scaled with the gravitational time scale $\sqrt{R/g}$.

FIG. 3. Oscillation frequencies computed from the full linearized flow (4) and (5) for ($H/R = 0.276$; $m = 3$) as a function of ξ/R, scaled as in Fig. 2. Only the rightmost instability at ξ/R slightly above 0.3, the intersection of the shaded lines, is seen experimentally and corresponds to the one in the two-dimensional model at $\xi/R \approx 0.43$. The higher resonances are much narrower and weaker.

small. We also assume that we can find a solution ω of the coupled problem which is close to both, i.e., $\omega = \omega_c + \Delta$ where Δ is also small. Inserting into (11) and expanding to lowest order in the small quantities, we find $\Delta^2 - \epsilon\Delta - K = 0$, where

$$K = \frac{m^2 g g_c}{\xi R} \frac{(F^2 - 1)}{D_c'(\omega_c)D_g'(\omega_g)}. \qquad (15)$$

Thus, Δ becomes complex if $|\epsilon| < 2|K|^{1/2}$ and $K < 0$. From (12), it is clear that $F > 1$, and thus instability [Figs. 2(d) and 2(c)] requires that $D_c'(\omega)D_g'(\omega) < 0$, i.e., $mU(R)/R < \omega < mU(\xi)/\xi$, showing that the gravitational waves run forward and the centrifugal waves run backward with respect to the local mean flow. Since their velocity must coincide at resonance, the mean flow must be slower than the wave speed at $r = R$ and quicker than the wave speed at $r = \xi$. In Cairns terminology, the centrifugal wave has negative energy.

To support this simple model, we have solved the set of equations (4) and (5) for the full linearized flow numerically using the finite element software FreeFem++ [9]. Figure 3 shows the eigenvalues (frequencies) with the same set of parameters as in Fig. 2. The full solution allows for many more wave types, but as seen in the figure they still organize into two families, with dispersion relations like gravity waves and like centrifugal waves, respectively. A number of unstable and stable resonances are observed. The resonance leading to the highest growth rate occurs between the waves with the simplest structure in each family and is well captured by the simple 2D model.

To compare our simple modeling with the experiments of Ref. [2], we need to relate the parameters of the fluid state, say, ξ and Γ, to the control parameters of the

experiment, namely, the filling height H and the bottom plate rotation rate f. This is a somewhat difficult task because the boundary layers neglected so far will become important near the plate and the wall. To simplify, we proceed by thinking of the fluid body as a conduit for angular momentum: The fluid will tend to settle in a state where the inflow of angular momentum equals the outflow. We model the turbulent flow by Prandtl's mixing length theory [10], where the shear stress acting on the fluid at the walls is $\sigma \approx \rho|\Delta u|\Delta u$ and Δu is the difference between the velocities of the solid boundary and of the free stream flow. The torque acting on the fluid over a boundary area $\mathcal{A}$ is proportional to $\int d\mathcal{A}\,r\sigma$. Setting the accelerating torque from the fast bottom plate equal to the decelerating torque from the stationary side wall, we obtain the equilibrium criterion [11]

$$\int_\xi^R dr[(r^2/x^2) - 1]|(r^2/x^2) - 1| = \zeta, \qquad (16)$$

where $x \equiv (2\pi)^{-1}\sqrt{\Gamma/f}$. For given ξ and ζ, we look for a solution for x, which then, via (2) and (3), links the bottom frequency f to the flow parameters. In Fig. 4(a), we have superimposed the regions of instability in the $H - f$ plane for $m = 2$ to 6 for the two-mode model (11) with the experimental phase diagram. Considering the simplicity of the model, the agreement with the experiment is surprisingly good. For comparison, we show in Fig. 4(b) the analog result for the global model (4) and (5), which also agrees rather well, but with the instability regions shifted slightly downward in frequency. Here, we include only the mode with the simplest structure for each m, since the others are much narrower and weaker. The caveats in both the experimental data and the modeling by (16) are discussed in the Supplemental Material [11]. Note that we have instabilities of any order m, although
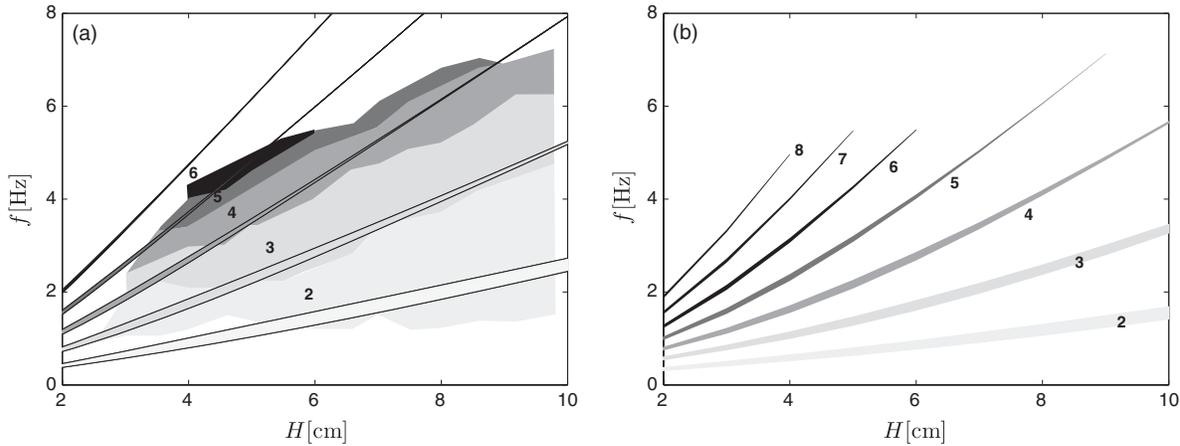
FIG. 4. Phase diagram showing the state as function of filling height H in cm and the bottom rotation rate f in Hz corresponding to a cylinder radius of $R = 14.5$ cm. The shades of grey (going from light grey to black) indicate polygons with $m = 2, 3, 4, 5, 6$. (a) Phase diagram from data given in Ref. [2] superimposed with regions of instability for the 2D model using (16). (b) Regions of instability from the full linearized flow (4) and (5) using (16), including only the simplest unstable mode at each m.

the resonances become very narrow for large order. This seems in disagreement with Ref. [12], where the polygons are viewed as rotating bound states of point vortices, and thus, due to theorems of Thomson and Havelock, should only be stable for $m < 7$. Our analysis is, however, restricted to small perturbations around the circular state, and therefore we cannot say whether the final nonlinear states would have secondary instabilities for large m. Note also that we cannot rule out the existence of polygons outside the narrow strips of instability in Fig. 4, since this could be caused by subcritical bifurcations. Indeed, a considerable hysteresis is observed experimentally [2,5].

We have seen that a potential vortex flow in a closed cylindrical container is unstable to perturbations with azimuthal wave numbers $m \geq 2$, and that the instability can be interpreted as a resonance between gravity waves
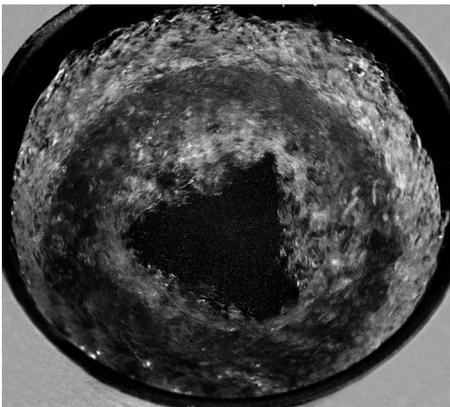
FIG. 5. A rotating triangle formed by stirring liquid nitrogen in a hot kitchen pot. Polygons with $m = 2, \ldots, 6$ are observed during the spin-down process, starting with the $m = 6$. The bottom of the pot is Teflon, which gives some unwanted reflections in the dark triangle.

propagating on the upper surface and centrifugal waves propagating on the inner surface. Such instabilities involving the interaction of different families of waves are not uncommon and have been described in various contexts, ranging from plasma dynamics and geophysical flows to astrophysics [13]. In our modeling, the occurrence of the polygon instability is linked to the simple potential vortex flow and should thus be rather general. This has led us to speculate if the instability may occur in a similar flow with different boundary conditions. The setup is simple: Place an ordinary kitchen pot on a hot stove and fill in a layer of liquid nitrogen. The temperature of the pot can be kept so high that the nitrogen undergoes film boiling at the solid boundary. The resulting gas layer lubricates the boundary and allows the liquid to flow almost unimpeded. By stirring rapidly with a spoon, one can induce a flow close to that of a potential vortex. As the liquid slowly spins down, one observes a series of polygons, starting from high m and evolving toward lower m. Depending on the initial conditions, one can obtain a larger or smaller part of the sequence $m = 6, 5, \ldots, 2$ during a single spin-down process, until the fluid settles into an approximately quiescent state, filling the entire bottom. Figure 5 shows a "triangle" obtained in this way, and movies of the spin-down process are provided in the Supplemental Material [11]. They correspond roughly to moving downward and slightly to the left in Fig. 4. It is surprising that one can observe the polygon states even in a flow set into rotation in a rather crude way and being disturbed by violent boiling. This supports our assumption that the boundary layers have little significance for the occurrence of polygons, which appears to be a robust wave-coupling phenomenon.

[1] G. H. Vatistas, J. Fluid Mech. **217**, 241 (1990).

[2] T. R. N. Jansson, M. P. Haspang, K. H. Jensen, P. Hersen, and T. Bohr, Phys. Rev. Lett. **96**, 174502 (2006).

[3] R. Bergmann, L. Tophøj, T. A. M. Homan, P. Hersen, A. Andersen, and T. Bohr, J. Fluid Mech. **679**, 415 (2011); **691**, 605 (2012).

[4] L. Tophøj and T. Bohr, J. Fluid Mech. **721**, 28 (2013).

[5] T. Suzuki, M. Iima, and Y. Hayase, Phys. Fluids **18**, 101701 (2006).

[6] G. H. Vatistas, J. Wang, and S. Lin, Acta Mech. **103**, 89 (1994).

[7] R. A. Cairns, J. Fluid Mech. **92**, 1 (1979).

[8] More precisely, for gravity waves, (9) is replaced by $\phi_c|_B = 0$, and, for centrifugal waves, (10) is replaced by $\phi_g|_A = 0$. Physically, this means that the free surface condition is replaced by a constant pressure condition at either A or B. Other choices, such as nonpenetration, are also possible, but the present one makes the mathematical analysis more straightforward.

[9] http://www.freefem.org/ff++/.

[10] H. Schlichting and K. Gersten, *Boundary Layer Theory* (Springer, New York, 2000).

[11] See Supplemental Material at http://link.aps.org/supplemental/10.1103/PhysRevLett.110.194502 where the derivation and limitations of Eq. (16) are discussed and videos of the spin-down process in liquid nitrogen are presented.

[12] G. H. Vatistas, H. A. Abderrahmane, and M. H. K. Siddiqui, Phys. Rev. Lett. **100**, 174503 (2008).

[13] S. Sakai, J. Fluid Mech. **202**, 149 (1989); R. S. MacKay and P. G. Saffman, Proc. R. Soc. Edinburgh, Sect. A **406**, 115 (1986); P. S. Joarder, V. M. Nakariakovet, and B. Roberts, Sol. Phys. **176**, 285 (1997).